

## Supporting Information

### **Deterministic Growth of Sodium Metal Anode on Pre-patterned Current Collector for Highly Rechargeable Seawater Battery**

Jaeho Jung,<sup>‡</sup><sup>a</sup> Daeyeon Hwang,<sup>‡</sup><sup>a</sup> Imanuel Kristanto,<sup>a</sup> Sang Kyu Kwak,<sup>\*a</sup> Seok Ju Kang<sup>\*a</sup>

<sup>a</sup>Department of Energy Engineering, School of Energy and Chemical Engineering, Ulsan National Institute of Science and Technology (UNIST), Ulsan 44919, Korea

\*E-mail: skkwak@unist.ac.kr, sjkang@unist.ac.kr

## Computational Section

### Modeling and Energy Calculations

Density functional theory (DFT) calculations were carried out using a computer program, Cambridge Serial Total Energy Package (CASTEP), to elucidate the dependence of Na metal plating on the surface of various current collectors.<sup>1</sup> First, we calculated the surface energy of the (001), (101), and (111) surfaces of each metal as shown in Fig. S11. Based on the calculated values (Fig. S12), the surface energy of the (111) surfaces are noticeably much higher than those of the (001) and (101) surfaces. Thus, we finalized our interface candidates to the (001) and (101) surfaces. Between these two surfaces, the (001) surface shows the lowest lattice mismatch across all metal current collector interfaces with Na; therefore, we constructed five interfaces between Na and each metal current collector based on its (001) surface (Fig. 1c). The in-plane strain to match the two parts in the interface structure was kept below 5%. Generalized gradient approximation (GGA) with the Perdew–Burke–Ernzerhof (PBE) functional was adopted for all calculations.<sup>2</sup> The ultrasoft pseudopotential was used to treat unreactive core electrons, and the energy cutoff was set to 550 eV.<sup>3</sup> The Broyden–Fletcher–Goldfarb–Shanno (BFGS) algorithm and Two-Point Steepest Descent (TPSD) algorithm were used for optimization of the geometry of the bulk systems and interface systems, respectively.<sup>4,5</sup> The convergence thresholds for geometry optimization and SCF density convergence were  $1 \times 10^{-5}$  eV atom<sup>-1</sup> and  $1 \times 10^{-6}$  eV atom<sup>-1</sup>, respectively. The convergence precision of geometry optimization for the maximum force, displacement, and maximum stress were set to 0.03 eV Å<sup>-1</sup>, 0.001 Å, and 0.05 GPa, respectively. For optimization of the bulk structure, a Monkhorst–Pack *k*-point mesh was used, and it was set to  $12 \times 12 \times 12$  for the bulk unit cell of Na, Au, Ag, Cu, Al, and Ni.<sup>6</sup>

The energy calculations employed in the study were adopted from the calculations carried out by Liu. et al., and Wang et al.; modifications were made before we carried out our calculations.<sup>7,8</sup> In this study, the interface formation energy ( $E_{if}$ ) of the interface system between sodium metal (Na) and the metal current collector (M) is defined as the energy difference between the total energy of the relaxed interface system and the energy of fully relaxed pure components.  $E_{if}$  can be calculated as follows:

$$E_{if} = E_{Na/M} - N_{Na} E_{Na} - N_M E_M,$$

where the total energy of the fully relaxed interfacial model (with  $N_{Na}$  units of Na and  $N_M$  units of M) is denoted by  $E_{Na/M}$ .

The energy per unit of the fully relaxed free pure Na and M bulk structures is denoted by  $E_{Na}$  and  $E_M$ , respectively. The interface formation energy defined based on this relation contains contributions from both the interfacial energy and elastic strain energy arising from the lattice mismatch between Na and the metal. The surface energies of pure sodium and metal were calculated based on the slab method by subtracting the total energy of the pure metal slab structure from the

bulk system energy with the same number of atoms. The interaction between the surfaces of the slab can be disregarded because the slab thickness (10 Å) is sufficiently large. This can be represented by the following relationship:

$$\gamma = \frac{1}{2S}(E_{\text{slab}}^N - N \times E_{\text{bulk}})$$

where the total energy of  $N$  units of the relaxed slab is denoted by  $E_{\text{slab}}^N$ , while the unit bulk total energy is expressed by  $E_{\text{bulk}}$ , the surface is denoted by  $S$ , and the coefficient 2 is used here because there are two equivalent surfaces in the surface model. The surface energy of each pure metal surfaces is shown in Fig. S12.

### Interfacial Energy

As discussed in the preceding section, the interface formation energy can be separated into two contributions, namely interfacial energy and strain energy. In order to evaluate the interfacial energy, the following procedures were utilized. The interface structures were subjected to full relaxation (atomic coordinates and cell-vector relaxations) to their external stress-free states, where  $E_{\text{Na/M}}$  can be obtained. Subsequently, both Na and M bulk structures with the same shape and comparable atomic layer numbers, as used in the full relaxation step, were subjected to relaxation in the normal ( $z$ ) direction (i.e., the in-plane ( $x$  and  $y$ ) lattice parameters were kept fixed). Then, the interfacial energy was calculated through the following equation:

$$\sigma_{\text{Na/M}}^{\text{int}} = \frac{E_{\text{Na/M}(xyz)} - N_{\text{Na}}E_{\text{Na}(z)} - N_{\text{M}}E_{\text{M}(z)}}{2S}$$

where the fully-relaxed total energy of the interfacial structure is expressed by  $E_{\text{Na/M}(xyz)}$ . While the energy per atomic layer of the pure Na and M bulk structures after constrained relaxation, along the interface normal direction ( $z$  direction) with fixed  $x$  and  $y$  components of lattice parameters, is expressed by  $E_{\text{Na}(z)}$  and  $E_{\text{M}(z)}$ , respectively. The atomic layer numbers of Na and M in the interfacial supercell is denoted by  $N_{\text{Na}}$  and  $N_{\text{M}}$ , respectively.

The work of adhesion ( $W_{\text{ad}}$ ) of the interface is defined as the amount of energy required to separate the two surfaces from the interface reversibly.<sup>9</sup> It can be calculated by subtracting interfacial energy from the two surfaces energy, as shown in the following relationship:

$$W_{\text{ad}} = \gamma_{\text{Na}} + \gamma_{\text{M}} - \sigma_{\text{Na/M}}$$

where  $\gamma_{\text{Na}}$  and  $\gamma_{\text{M}}$  denote the surface energies of Na and M from pure sodium and metal structure, respectively.  $\sigma_{\text{Na/M}}$  is defined as the interfacial energy of sodium and metal interface.

**Binding Energy:** We constructed each metal pure surfaces and introduced Na atom at similar distance on each metal surface (Fig. S1). Binding energy ( $E^b$ ) between Na atom with each metal surfaces were calculated based on the following equation:

$$E_b = E_{\text{Na(1)/M}} - E_{\text{Na(1)}} - E_M,$$

where  $E_{\text{Na(1)/M}}$ ,  $E_{\text{Na(1)}}$ , and  $E_M$  are total energies of the Na-adsorbed metal surface, isolated Na atom, and metal surface, respectively.

### Supplementary Note I.

For the Na/Ni interface based on the thin film model that we adopt for our DFT calculation, it showed high  $W_{\text{ad}}$  but low  $E_b$ . This contrasting result can be attributed to the nature of Ni metal. Ni metal possesses high surface energy (Fig. S12), this causes Na metal deposition on Ni surface to adopt island like formation (Fig. S13). The thin film model which we imposed during our calculation limits the relaxation of Na metal on Ni substrate, thus resulting into higher surface energy than it supposed in the island deposition model. Assuming to take into account the natural behavior of Na metal deposition on Ni surface, the surface energy of Na island is lowered that the that of thin film as it is thermodynamically more favorable. Additionally, according to the island growth model criteria,

$$\gamma_{\text{Ni}} < \gamma_{\text{Na}} + \sigma_{\text{Na/Ni}},$$

where  $\gamma_{\text{Ni}}$  is the surface energy of Ni metal (substrate),  $\gamma_{\text{Na}}$  is the surface energy of Na metal (crystal), and  $\sigma_{\text{Na/Ni}}$  is the interfacial energy of Na/Ni interface. Thus, the range of interfacial energy of Na/Ni interface can be expressed as follows:

$$\sigma_{\text{Na/Ni}} > (\gamma_{\text{Ni}} - \gamma_{\text{Na}}).$$

Based on above equation and using the calculated surface energies of pure Na and Ni, the minimum interfacial energy was estimated to be  $\sigma_{\text{Na/Ni}} = 13.05 \text{ eV nm}^{-2}$ . By taking the limit of a Na atom bound on Ni surface as the lowest possible  $W_{\text{ad}}$ , the  $W_{\text{ad}}$  range of Na on Ni was calculated to be  $0.06 \text{ eV nm}^{-2} < W_{\text{ad}} < 2.25 \text{ eV nm}^{-2}$ , as shown in Fig. 1c.

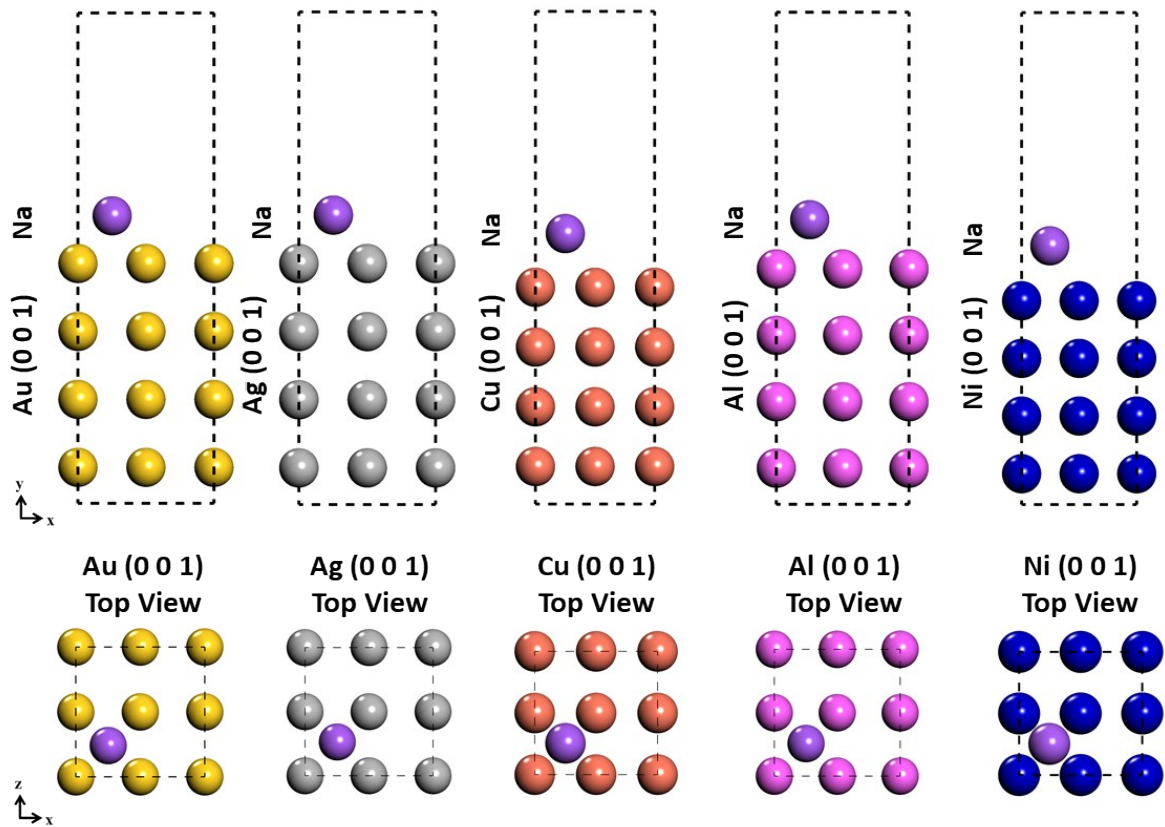


**Fig. S1** Model of system for calculating the binding energy of Na on each metal's (001) surface. The violet, gold, light gray, orange, pink, and blue spheres represent Na, Au, Ag, Cu, Al, and Ni atoms, respectively.

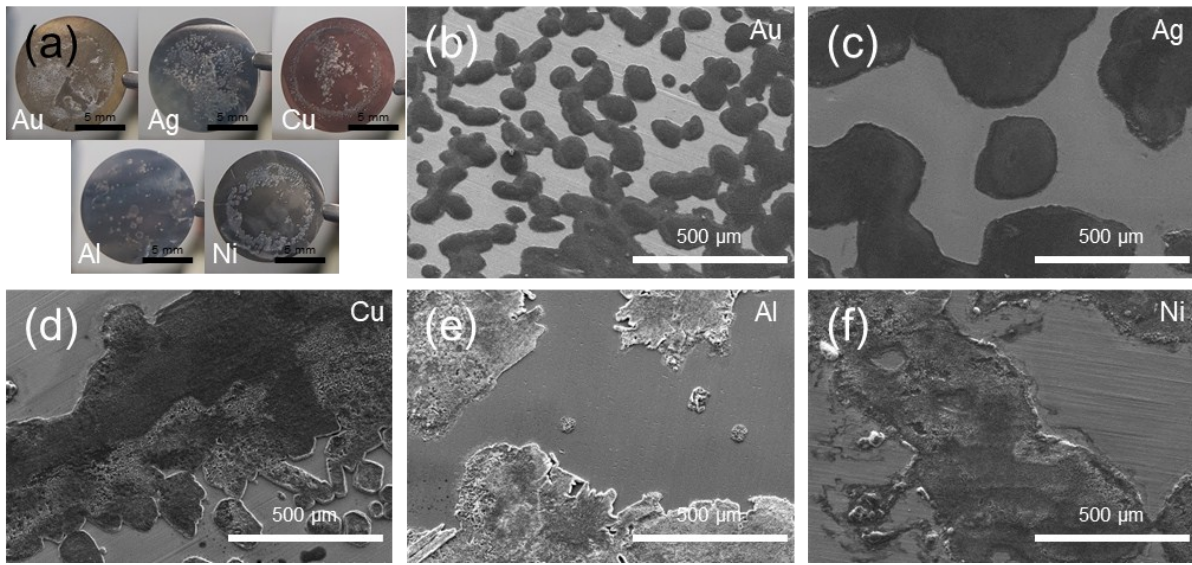


**Fig. S2** (a) Photographs and (b–f) plane-view SEM images of Au, Ag, Cu, Al, and Ni current collectors after plated with  $0.1 \text{ mAh cm}^{-2}$  Na metal.

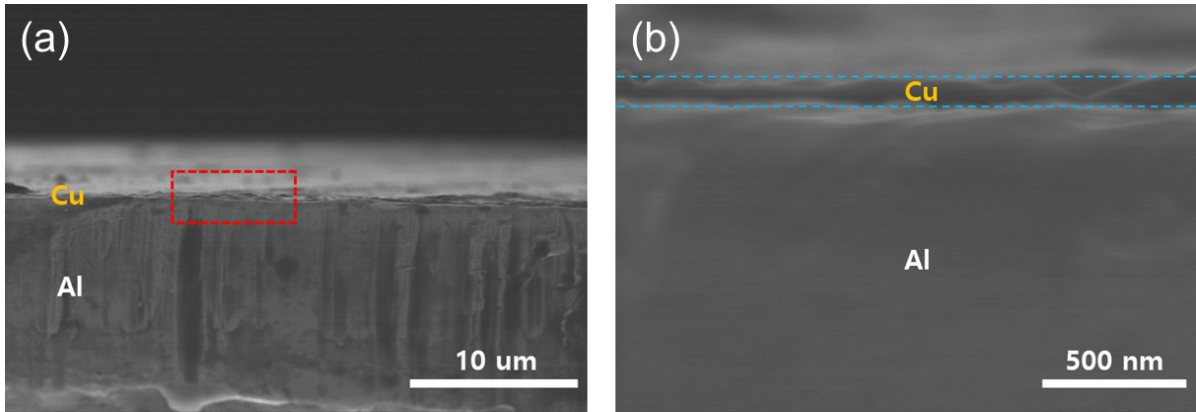


**Fig. S3** (a) Cross-sectional view SEM image of Cu/Al pre-patterned current collector. (b) Magnified SEM image of dash-dot square region in (a).

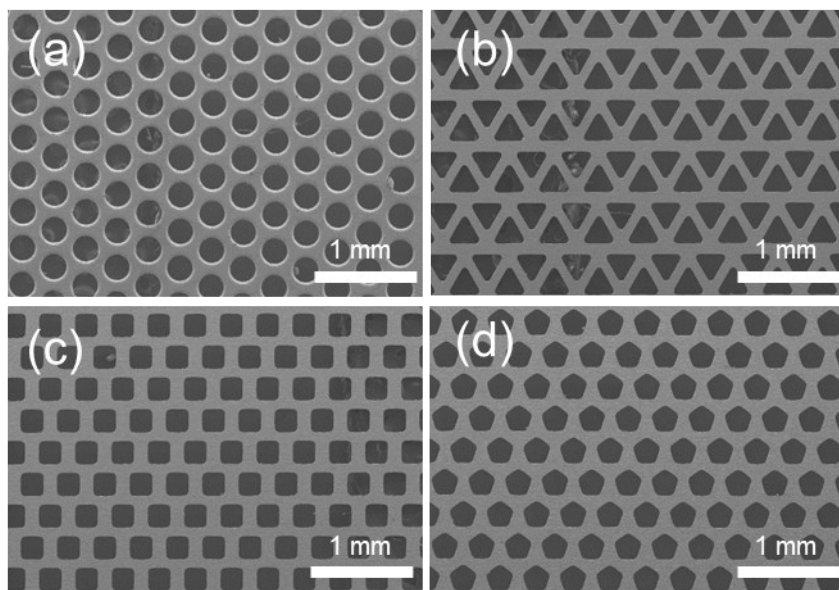


**Fig. S4** Plane-view SEM images of SUS masks with (a) circular, (b) triangular, (c) square, and (d) pentagonal patterns.



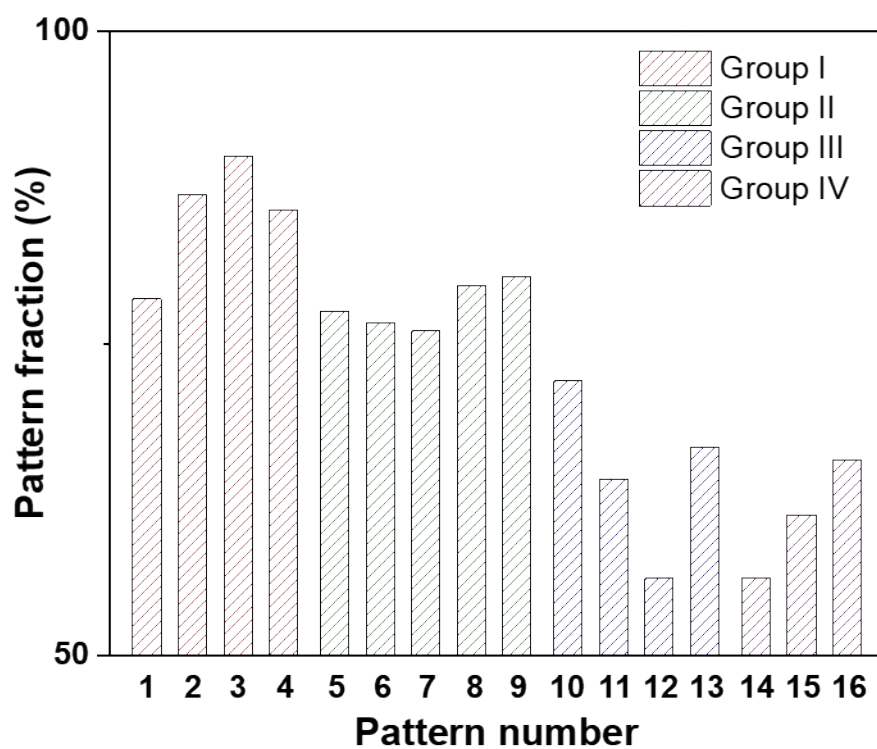


**Fig. S5** Histograms of pattern fraction of Na metal islands versus various pre-patterned current collectors shown in Table S1.

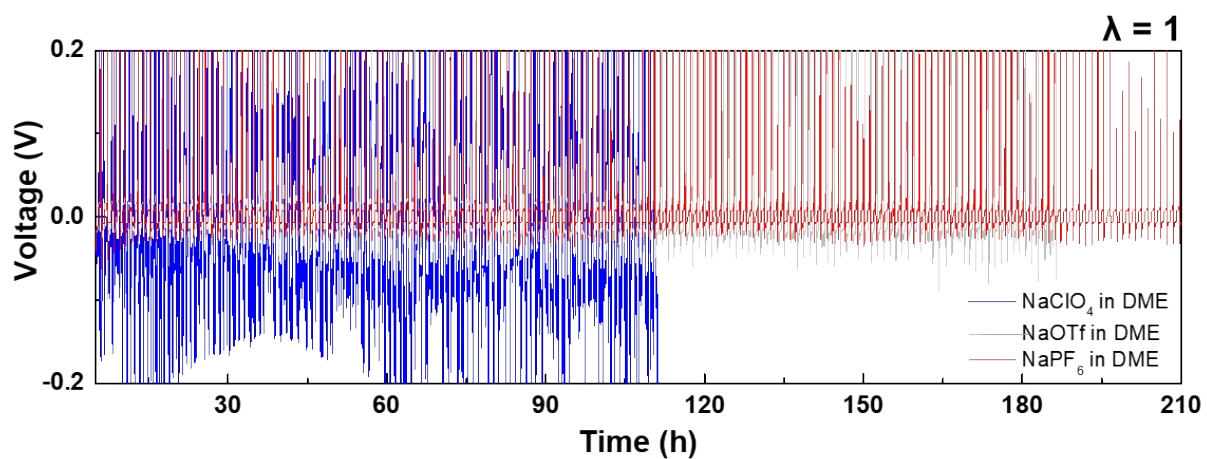


**Fig. S6** Galvanostatic plating and stripping on pre-patterned current collectors ( $\lambda=1$ ) with 1 M NaClO<sub>4</sub>-DME (blue), 1 M NaOTf-DME (gray), and 1 M NaPF<sub>6</sub>-DME (red) electrolytes.

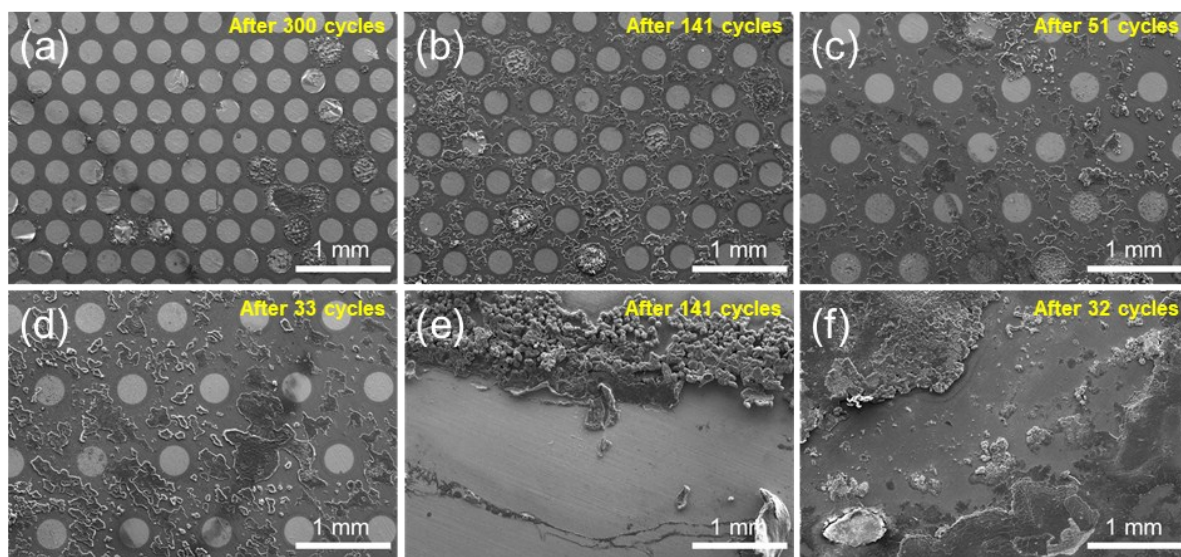


**Fig. S7** Post-mortem SEM images of pre-patterned Cu/Al current collectors with  $\lambda$  values of (a) 0.5, (b) 1, (c) 1.5, and (d) 2, (e) pristine Cu, and (f) Al current collector after cycling tests of 2032-type coin cells.

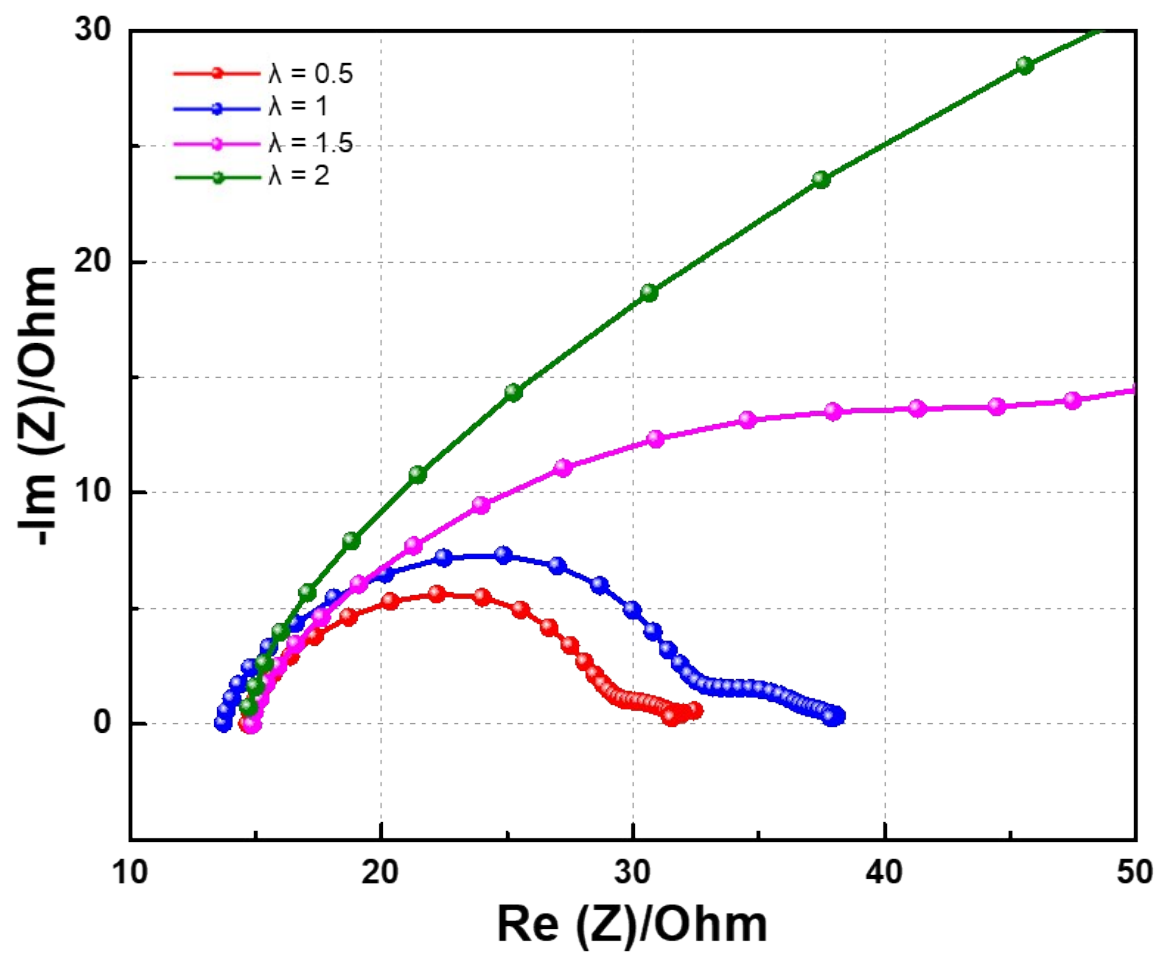


**Fig. S8** Nyquist plots of the impedance spectra for Cu/Al patterns with  $\lambda$  value range of 0.5-2.0 at the 15<sup>th</sup> cycle.

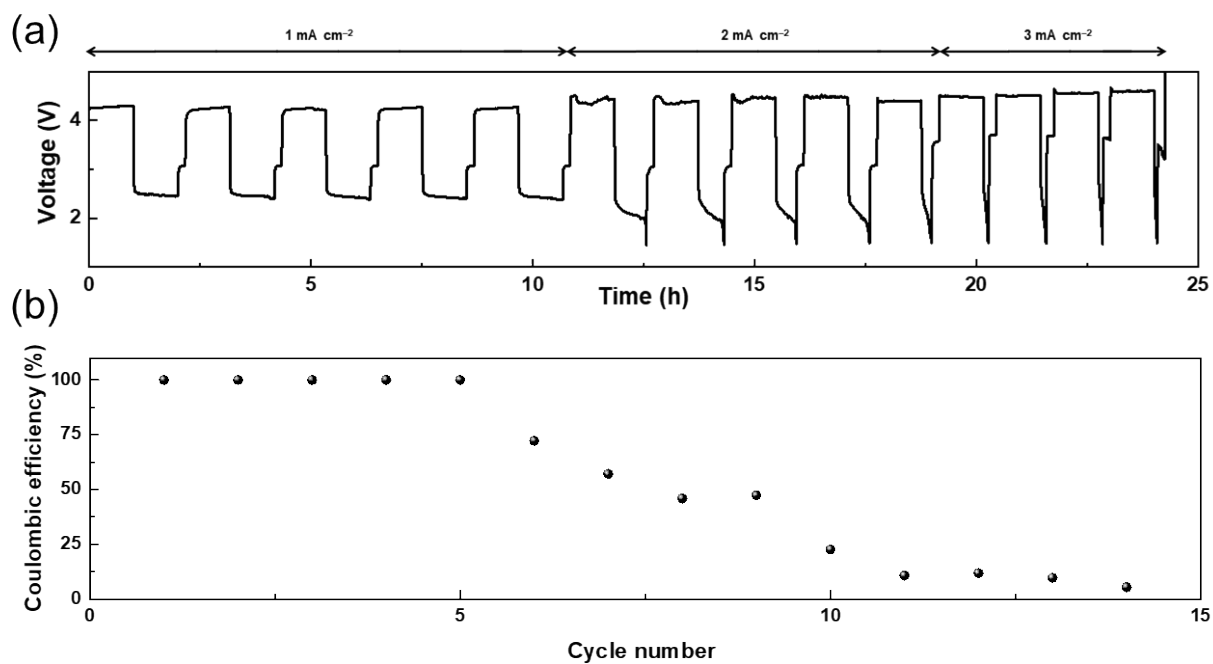


**Fig. S9** (a) Rate performance and (b) corresponding Coulombic efficiency of Cu/Al pre-patterned current collector containing seawater battery in the current density range of 1 to 3 mA cm<sup>-2</sup>.

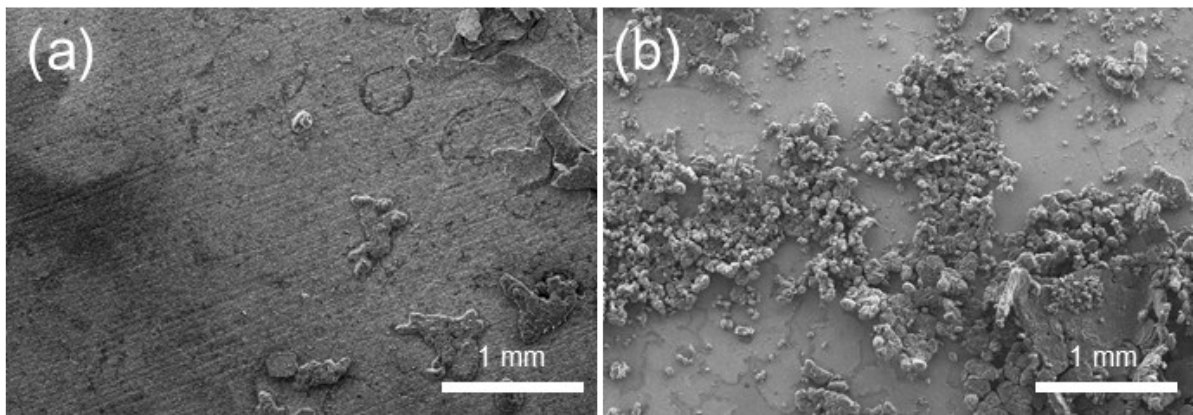


**Fig. S10** Plane-view SEM images of (a) NASICON and (b) pristine Cu foil surfaces with Cu foil after 57 cycles.

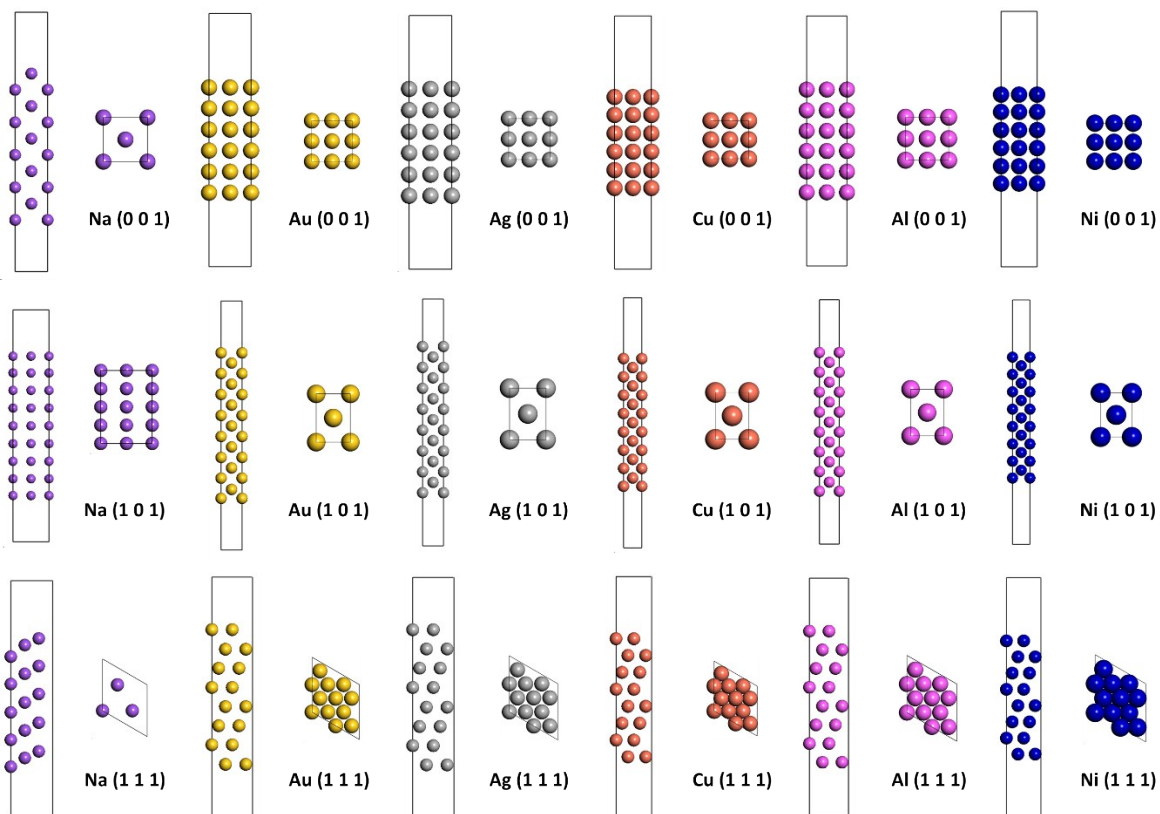


**Fig. S11** Surface models of Na, Au, Ag, Cu, Al and Ni current collectors with (001), (101), and (111) surfaces.

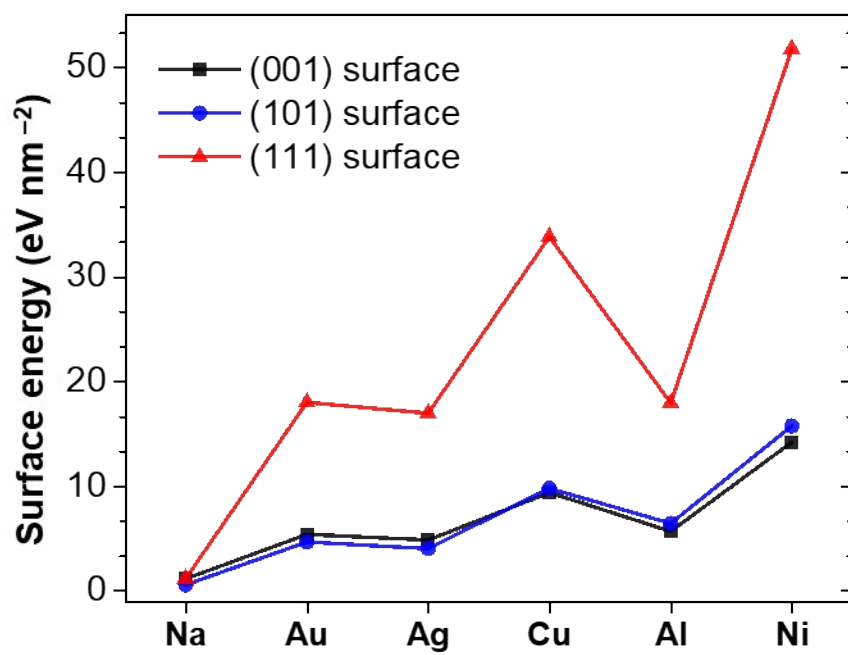


**Fig. S12** Surface energy of (001), (101), and (111) surfaces of pure metal systems.



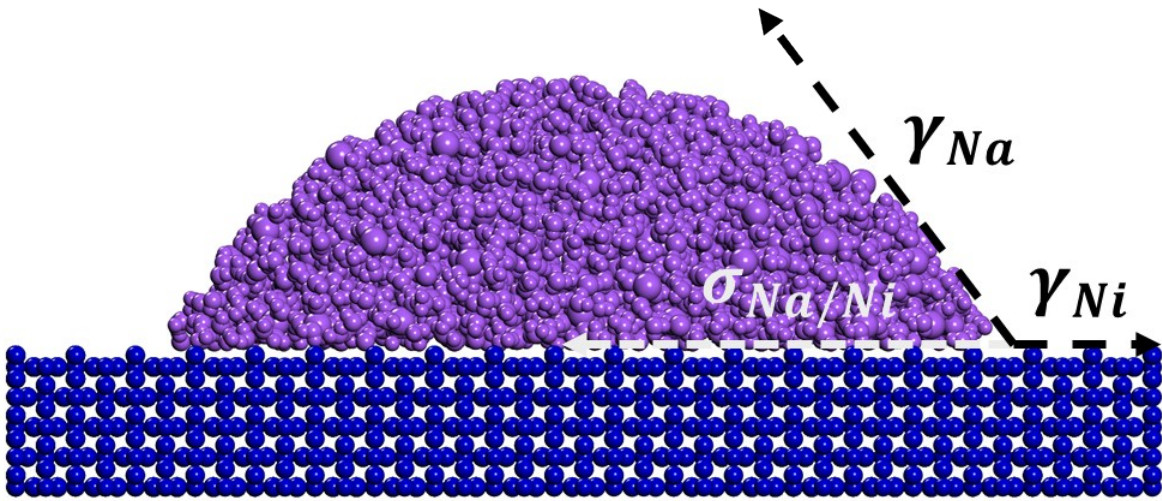


**Fig. S13** Island growth of Na metal deposition on Ni metal surface.  $\gamma_{Ni}$  is the surface energy of Ni metal (substrate),  $\gamma_{Na}$  is the surface energy of Na metal (crystal), and  $\sigma_{Na/Ni}$  is the interfacial energy of the Na/Ni interface.

	Group I				Group II					Group III				Group IV		
Pattern #	1	2	3	4	5	6	7	8	9	10	11	12	13	14	15	16
Pattern diameter ( <i>r</i> ) [μm]	150	200	250	300	100	150	200	250	300	100	200	250	300	200	250	300
Pattern distance ( <i>d</i> ) [μm]	100	100	125	150	100	150	200	250	300	150	300	375	450	400	500	600
$\lambda$ [ <i>d/r</i> ]	0.66	0.5	0.5	0.5	1	1	1	1	1	1.5	1.5	1.5	1.5	2	2	2
Pattern fraction [%]	78.6	86.9	90	85.7	77.6	76.7	76	79.7	80.4	72	64.1	56.2	66.7	56.2	61.3	65.7

a) Pattern fraction = (Number of Na deposited patterns / Number of total pre-patterns) × 100

**Table S1.** Pattern fraction of Na metal islands on various pre-patterned current collectors.

## References

- 1 S. J. Clark, M. D. Segall, C. J. Pickard, P. J. Hasnip, M. I. Probert and K. Refson, *Z. Kristallogr. Cryst. Mater.*, 2005, **220**, 567.
- 2 J. P. Perdew, K. Burke and M. Ernzerhof, *Phys. Rev. Lett.*, 1996, **77**, 3865.
- 3 D. Vanderbilt, *Phys. Rev. B*, 1990, **41**, 7892.
- 4 C. G. Broyden, *IMA J. Appl. Math.*, 1970, **6**, 76.
- 5 J. Barzilai and J. M. Borwein, *IMA J. Numer. Anal.*, 1988, **8**, 141.
- 6 H. J. Monkhorst and J. D. Pack, *Phys. Rev. B*, 1976, **13**, 5188.
- 7 Z. Liu, Y. Qi, Y. X. Lin, L. Chen, P. Lu and L. Q. Chen, *J. Electrochem. Soc.*, 2016, **163**, A592.
- 8 Y. Wang, Z.-K. Liu, L.-Q. Chen and C. Wolverton, *Acta Mater.*, 2007, **55**, 5934.
- 9 M. Benoit, C. Langlois, N. Combe, H. Tang and M.-J. Casanove, *Phys. Rev. B*, 2012, **86**, 075460.